Egyptian Journal of Petroleum (2013) 22, 373–380

Egyptian Petroleum Research Institute

Egyptian Journal of Petroleum

www.elsevier.com/locate/egyjp
www.sciencedirect.com

FULL LENGTH ARTICLE

Selective nano alumina supported vanadium oxide catalysts for oxidative dehydrogenation of ethylbenzene to styrene using CO_2 as soft oxidant

A.M. Elfadly [a], A.M. Badawi [a], F.Z. Yehia [a], Y.A. Mohamed [b], M.A. Betiha [a], A.M. Rabie [a,*]

[a] Egyptian Petroleum Research Institute, Nasr City, Cairo, Egypt
[b] Faculty of Science Al Azhar University, Nasr City, Cairo, Egypt

Received 14 October 2012; accepted 11 December 2012
Available online 5 December 2013

KEYWORDS

Dehydrogenation;
Styrene;
CO_2;
γ-Al_2O_3;
Catalysis

Abstract Nano alumina-supported V_2O_5 catalysts with different loadings have been tested for the dehydrogenation of ethylbenzene with CO_2 as an oxidant. High surface area nano-alumina was prepared and used as support for V_2O_5 as the catalyst. The catalysts were synthesized by impregnation techniques followed by calcinations and microwave treatment, denoted as V_2O_5/γ-Al_2O_3-C and V_2O_5/γ-Al_2O_3-MW, respectively. The V_2O_5 loading was varied on nano-alumina from 5 to 30 wt%. The support and catalysts were characterized by X-ray diffraction (XRD), Barett–Joyner–Halenda (BJH) pore-size distribution, N_2-adsorption isotherms, Fourier transform infrared (FT-IR), scanning electron microscopy (SEM), transmission electron microscopy (TEM) and temperature programed desorption (TPD-NH_3). The characterization results indicated that V_2O_5 is highly dispersed on alumina up to 30%-V_2O_5/γ-Al_2O_3-MW prepared by MW method. The TPD studies indicated that there are significant differences in acid amount and strength for V_2O_5/γ-Al_2O_3-C and V_2O_5/γ-Al_2O_3-MW-catalysts. The catalytic activity of the prepared catalysts was evaluated in the temperature range 450–600 °C in relation to the physicochemical properties and surface acidity. The results revealed that optimum catalytic activity and selectivity (~100%) toward styrene production were obtained using 10% V_2O_5/γ-Al_2O_3-MW catalyst treated with microwave.

1. Introduction

The dehydrogenation of alkylbenzenes is a commercial process used for the production of alkenylbenzenes monomers such as divinylbenzene and styrene. The catalytic dehydrogenation of ethylbenzene to produce styrene, as a representative process, is performed in industry over promoted iron oxide catalyst in the presence of a large quantity of steam, at high tempera-

* Corresponding author. Tel.: +20 2 22747917; fax: +20 222747433.
E-mail addresses: mohamed_betiha@yahoo.com (M.A. Betiha), abdo3040@yahoo.com (A.M. Rabie).
Peer review under responsibility of Egyptian Petroleum Research Institute.

ELSEVIER Production and hosting by Elsevier

1110-0621 © 2013 Production and hosting by Elsevier B.V. on behalf of Egyptian Petroleum Research Institute.
Open access under CC BY-NC-ND license. http://dx.doi.org/10.1016/j.ejpe.2013.10.007

ture of 600–700 °C [1–4]. Since the process is equilibrium –limited and energy intensive, there is a great interest, recently, for the development of an alternative methodology. Thus, the use of CO_2, as a soft oxidant, in the selective catalytic oxydehydrogenation of ethylbenzene has been widely investigated [5–8]. The process should be energy saving and environmentally friendly in respect of utilization of CO_2 which is one of the greenhouse gases causing global warning, and the energy required is much lower [8]. In addition, CO_2 can decrease the partial pressure of reactants more effectively than steam and it has highest heat capacity among various typical gases (9, 10). Further, in the presence of CO_2, coupling between reverse water gas shift ($CO_2 + H_2 \leftrightarrow CO + H_2O$) and dehydrogenation reaction becomes more favorable [4,10–12].

Several catalysts exhibited high catalytic activity for the dehydrogenation of ethyl benzene in presence of CO_2 [6–9,13–16]. Among these catalysts, vanadia supported on alumina (VO_x/Al_2O_3) catalysts, were more stable and exhibited better performance for oxidehydrogenation of ethyl benzene with CO_2 [8,13–17].

On the other hand, it is well known that the physical and chemical properties of support have an important effect on catalytic activity [18,19]. Thus, high specific surface area helps the active component of catalysts to disperse well and is extremely beneficial in improving catalytic activity. In this respect, nano alumina particles with the features of large specific surface and high reactive activity are used as carriers for petroleum cracking catalysts [20]. The crystal phase, specific surface area, pore distribution and other physical–chemical properties of nano-alumina particles specific to the needs of catalytic reactions can be obtained by changing the preparation conditions of nano-alumina particles [21].

Herein, we report the preparation of nano alumina by two methods, conventional and microwave method. The prepared nano-alumina was used as support for V_2O_5 catalysts. The performance of prepared catalysts is discussed from different faces.

2. Materials and methods

2.1. Material preparation

Aluminum nitrate ($Al(NO_3)_3{\cdot}9H_2O$, 95%; Merck), sodium carbonate (Na_2CO_3, 98%; Merck) and deionized water were used as starting chemicals. $Al(NO_3)_3{\cdot}9H_2O$ (25 g, 0.066 M) solution and Na_2CO_3 (10.38 g, 0.125 M) solution were dissolved in 600 mL of deionized water, separately. Then Na_2CO_3 and $Al(NO_3)_3{\cdot}9H_2O$ solutions (from two separate burettes) were added drop by drop into a 2-L capacity round-bottom flask containing 60 mL of ethylene glycol dissolved in 400 mL of deionized water under stirring to precipitate Al^{3+} cations as hydroxides form. The pH of the solution was adjusted in the range of 7.5–9 using HNO_3 and/or NaOH (Merck, GR). The precipitate was aged at 70 °C for 3 h, filtered off and washed several times with water/ethanol (70/30; wt/wt) until solution free Na and NO_3 ions are obtained. The white precipitate was dried at 100 °C overnight and calcined in a programmable furnace at 550 °C with heating rate of 2 °C min^{-1} for 5 h in air to produce γ-Al_2O_3 powder [22].

A series of 5–30%VO_x@Al_2O_3 catalysts were prepared from solutions of ammonium metavanadate (NH_4VO_3; Merck, >99%) and oxalic acid (Alfa Products, UK). Thus, the obtained mixture was divided into two equal parts [5,6,27]:

Part I, required amount of NH_4VO_3 that gives 5–30% of V_2O_5 was dissolved in adequate amount of water in the presence of oxalic acid (NH_4VO_3/oxalic acid = 75.1 wt%). The solution was added to γ-Al_2O_3 powder with solution impregnation method. After 2 h the catalyst was heated to 80 °C under stirring to vaporize the excess water and then dried at 110 °C for 5 h. Finally, the mixture product was calcined in air at 600 °C with ramping rate of 2 °C/min for 5 h and the prepared catalysts are denoted as C1, C2, C3 & C4 for 5, 10, 20 & 30% V_2O_5/γ-Al_2O_3 respectively.

Part II, the previous solution of NH_4VO_3-oxalic acid mixture was precipitated on γ-Al_2O_3 with a ratio of 5–30% at ambient temperature under stirring for 2 h. Then the mixture was subjected to microwave energy radiation (300 W; 10 s on and 20 s off for 10 min) to obtain vanadium oxide supported on γ-Al_2O_3. After self-cooling of mixture, the catalyst was filtered off, dried at 50, 80, and 110 °C for 5, 5 and 2 h, respectively, and the prepared catalysts are denoted as MW1, MW2, MW3 & MW4 for 5, 10, 20 & 30% V_2O_5/γ-Al_2O_3 respectively.

2.2. Characterization methods

X-ray diffractograms were obtained on a XPERT X-ray diffractometer, operating with CuKα radiation (λ = 0.1542 nm) and X-ray radiation (X-ray generator current and voltage set at 40 mA and 45 kV). The diffractograms were recorded in the 2θ range of 4–80° with a 2θ step size of 0.01° and a step time of 10 s.

Fourier transform infrared spectroscopy (FTIR) measurements were performed using Nicolet IS-10 FTIR over the wave number 4000–400 cm^{-1}.

Nitrogen adsorption and desorption isotherms were measured at −196 °C on a NOVA 3200 system (USA). The samples were out gassed for 3 h at 300 °C under vacuum in the degas port of the adsorption analyzer. The specific surface area was calculated using the Brunauer–Emmett–Teller (BET) model. The pore size distributions were obtained from the desorption branch of the nitrogen isotherms by the Barrett–Joyner–Halenda (BJH) method.

Thermal stability was carried out in TA Instruments SDTQ 600 simultaneous TGA-DSC thermogravimetric analyzer. The analyses were conducted for a total sample mass of 10.0 ± 0.2 mg. The samples were heated under nitrogen flow (100 ml min^{-1}) from 50 to 750 °C, at 20 °C min^{-1}.

Transmission electron microscopy (TEM) images were recorded on a JEOL 2011 microscope (Japan) operated at 200 kV. Before TEM characterization, the samples were dispersed in ethanol. The suspensions of the samples were dropped on a holey carbon coated copper grid.

Scanning electron microscopy (SEM) pictures were determined on a JEOL JSM-6700F field emission scanning electron microscope.

Temperature programed desorption of ammonia (NH_3-TPD) was measured on a CHEMBET 3000 chemical absorber (Quantachrom). Before measurements, the samples were firstly activated at 500 °C for 1 h under helium atmosphere. After the temperature cooled down to 100 °C, the samples were swept by ammonia for 1.5 h, then the gas was switched into helium to remove the physically adsorbed ammonia molecules, until the baseline was flat. After this,

the temperature was increased to 500 °C with a ramping rate of 10 °C/min to obtain the NH_3-TPD curves.

3. Catalytic activity evaluation

The catalytic activity for vapor phase ODH of EB was investigated in a down flow fixed-bed stainless steel micro reactor. For each run, 2 g of sample was loaded in the reactor with 2 g of glass beads. The reactor was heated to 600 °C at a rate of 10 °C/min in the flow of N_2 gas (20 mL/min) and kept at this temperature for 2 h then N_2 was replaced with CO_2 gas (20 mL/min). The catalyst pretreatment was continued at 600 °C for 1 h with CO_2 (20 mL/min) before conducting the reaction. The EB was passed through the preheating zone of the reactor using liquid feed pump (Gilson 307) with a constant feed rate of 1.0 ml/h. Gaseous and liquid products were analyzed simultaneously by gas chromatography (agilent 7890) equipped with TCD and FID. For analysis of liquid products, HP 5 capillary column (30 m, 0.32mmi.d. and 0.25 μm film thickness) was employed and for gaseous products Porapak Q 80/100 column (6 ft × 1/8 in.) was used. The main gaseous products detected were hydrogen, ethylene, methane, carbon monoxide and carbon dioxide. The main liquid products detected were Styrene, ethylbenzene, benzene and toluene.

4. Results and discussions

4.1. Physico-chemical characterization

FTIR spectra of all vanadium oxide loaded alumina are shown in Fig. 1. In nano alumina, the vibrations of Al–OH and Al–O bonds are observed at a range of 3000–3600 cm^{-1} and ~1632 corresponding to the stretching and bending vibration of hydrogen bonding OH groups, respectively [21]. The presence of bands in the region 2900–3600 cm^{-1} is related to lattice surface hydroxyl groups and may have resulted from the presence of moisture in the powder or KBr.

The stretching vibrations at ~1560 cm^{-1} are related to Al–OH bond. The weak bands between 1100 and 1200 cm^{-1} are related to Al–O [23]. The alumina band intensity at ~1100 cm^{-1} is diminished and moved toward red shift upon increasing V_2O_5 ratio. The red shift can result from increasing V_2O_5 particle size and consumption of alumina free OH-groups. The bands at ~500–800 cm^{-1} are characteristic of V–O–V vibrations, which are more pronounced in samples prepared by microwave than traditional method. These bands do not closely match those of crystalline V_2O_5 (which possesses sharp bands at 994, 702, 527 and 404 cm^{-1}), but the somewhat similar band positions suggest the structures of hydrated surface vanadium oxide on alumina and V_2O_5 [24]. Finally, a new band at 970 cm^{-1} appeared for microwave prepared sample due to molecular V=O supported alumina and its intensity increases with increasing vanadium loading.

Figs. 2 and 3 show the nitrogen physisorption measurements of prepared materials and the textural properties data are collected in Table 1. Alumina-free replicas show Type IV isotherms with a pronounced condensation step in the relative pressure (P/P_0) range of ~0.1–0.2, indicating narrow-sized mesopores [23]. The N_2-uptake of the adsorption isotherms at $P/P_0 > 0.8$ is associated with a second capillary condensation of nitrogen due to large voids between the particles. The presence of a hysteresis loop between the adsorption and desorption branches of meso-alumina indicates tubular pore structure or interconnected pores. After the introduction of V_2O_5, the type-IV isotherms with an H1-Type hysteresis loop

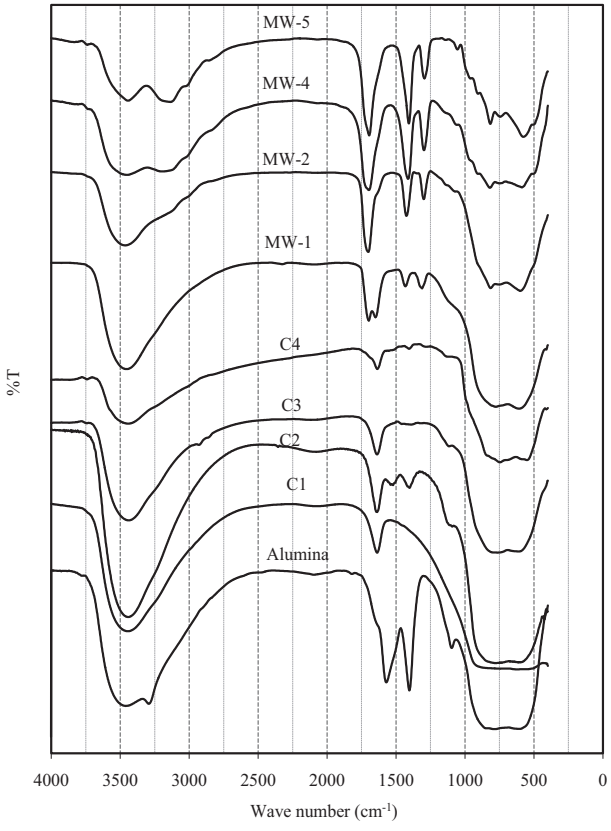

Figure 1 FTIR spectra of V_2O_5/-Al_2O_3 catalysts.

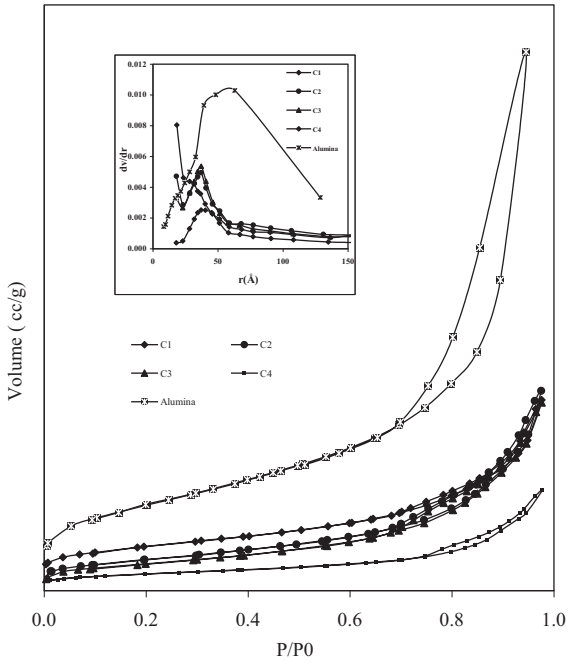

Figure 2 N_2 gas adsorption–desorption isotherms and pore size distribution of V_2O_5/γ-$A1_2O_3$-C.

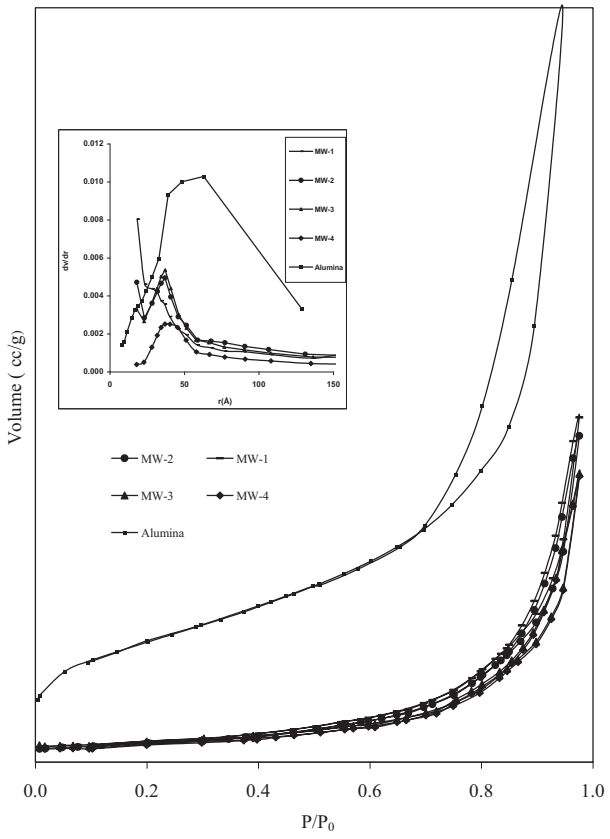

Figure 3 N_2 gas adsorption–desorption isotherms and pore size distribution of V_2O_5/γ-$A1_2O_3$-MW.

are still observed. However, a decrease in the value of surface area and pore volume was observed with increasing vanadium ratio. This is in accordance with the literature report [23,25]. The pore size distribution of prepared materials is shown in Figs. 2 and 3. It is clear that the pore width is shifted toward a lower value depending on the percent of V_2O_5. Nevertheless, pore sizes of all catalysts are still in a mesoporous scale demonstrating that there are no diffusion limitations during adsorption and catalysis because the molecular dimension of ethylbenzene is much smaller (6.1 Å) than the catalyst pore sizes (~37 Å) [13].

To confirm the presence of vanadium oxide nanoparticles in the pores of the alumina substrate, the normalized S_{BET} values were calculated using an equation proposed by Vradman et al. [26].

$$NS_{BET} = \frac{S_{BET} \text{ of the catalyst}}{(1-y) \times S_{BET} \text{ of the support}}$$

where NS_{BET} is normalized S_{BET} and y is the weight fraction of the active phases. The values of normalized NS_{BET} are also compiled in Table 1. These normalized surface areas of vanadium oxide catalyst value was <1 and $<<1$ for catalysts prepared by microwave and calcination methods, respectively. This value indicated some blocking of the support pores with vanadium oxide particles. The NS_{BET} values of the catalysts followed the order: MW1 > C1 > MW2 > MW3 > C2 > MW4 > C4 > C3. Also, one can conclude that in the samples prepared with microwave method materials, the vanadium oxide species were located on a low proportion in the internal support surface (pores) and high proportion in the external surface area ($NSBET \approx 0.5$), contrary to this, the supported vanadium oxide catalysts prepared with traditional method materials were located mainly blocking the pores (NSBET = 0.16).

XRD patterns of all V_2O_5/alumina are shown in Fig. 4. Li et al., [27] reported the reflections consistent with the layered structure of hydrated V_2O_5 at 2θ = 9.1, 18.3, 27.7, 37.2, and 46.0° are assigned to (001), (002), (003), (004), and (005) lattice planes, respectively. XRD shows absence of all previous peaks except 30%-VOx/Al_2O_3-C. In addition, XRD patterns of low loaded vanadium catalysts (< 30%) present only peaks due to alumina. The highest loaded vanadium catalysts (30% w/w), a weak peak is detected at 27° that could be ascribed to vanadate-like species [28]. The low intensity of this peak and the absence of new crystalline phases associated with vanadium can be explained either by the low concentration of such vanadate species or/and by assuming that they are dispersed on the catalyst surface.

Ammonia adsorption–desorption technique usually enables the determination of the amount and strength of acid sites present on the catalyst surface together with total acidity. The NH_3-TPD profiles of the catalysts with different V_2O_5 loadings in nano-alumina are shown in Fig. 5 and the data are presented in Table 1. Peri et al. reported that γ-alumina shows three types of OH groups [29]; (1) a terminal OH group attached to a single tetrahedral or octahedral Al ($OHAl_T$ or $OHAl_O$). (2) a bridging OH coordinated to two octahedral Al (OH_2Al_O) or to one tetrahedral Al and one octahedral Al ($OHAl_OAl_T$). (3) a bridging OH attached to three octahedral Al (OH_3Al_O), giving rise to acidic protons respectively.

Table 1 Textural properties of the prepared samples.

Samples	Surface area ($m^2\ g^{-1}$)	Average pore volume ($cm^3\ g^{-1}$)	Pore radius (Å)	NS_{BET}
γ-Al_2O_3	308.88	0.854	62.91	-
C1- 5% V_2O_5/γ-Al_2O_3	132.44	0.266	36.9	0.45
C2- 10% V_2O_5/γ-Al_2O_3	110.21	0.251	34.3	0.34
C3- 20% V_2O_5/γ-Al_2O_3	59.81	0.230	31.61	0.22
C4- 30% V_2O_5/γ-Al_2O_3	48.31	0.211	28.16	0.22
MW1- 5% V_2O_5/γ-Al_2O_3	155.56	0.337	37.31	0.53
MW2- 10% V_2O_5/γ-Al_2O_3	114.45	0.335	36.94	0.41
MW3- 20% V_2O_5/γ-Al_2O_3	99.31	0.317	36.11	0.40
MW4- 30% V_2O_5/γ-Al_2O_3	53.55	0.307	34.35	0.25

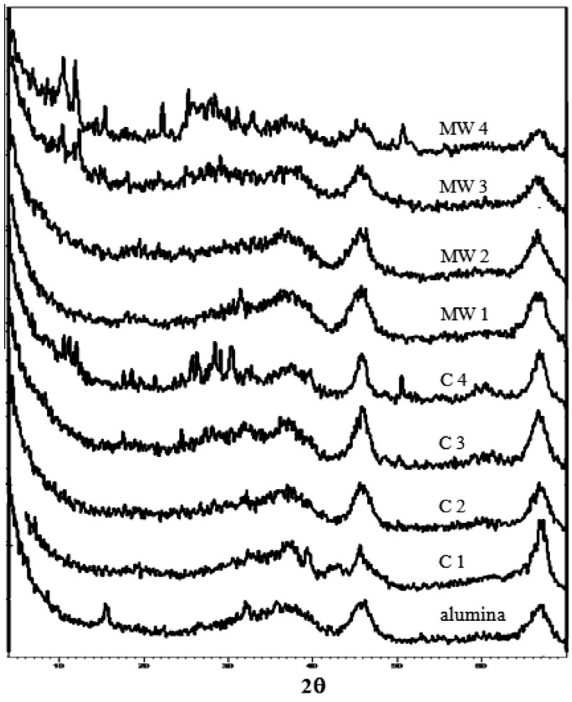

Figure 4 XRD patterns of Alumina, V_2O_5/Al_2O_3 (C) and V_2O_5/Al_2O_3 (MW).

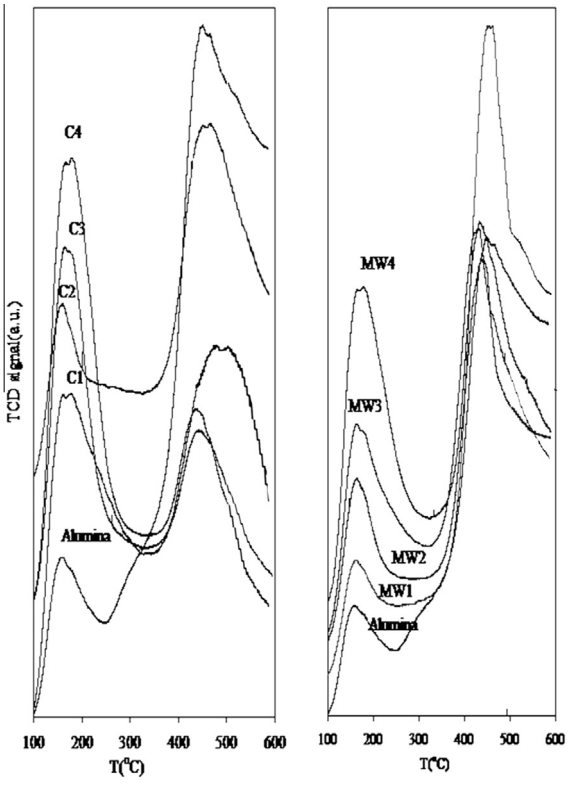

Figure 5 NH_3-TPD profiles of different prepared catalysts.

It can be seen that both acid amount and strength of V_2O_5 decrease with increasing V_2O_5 loadings up to 30%. Possibly, this behavior may be due to the coverage walls of the support

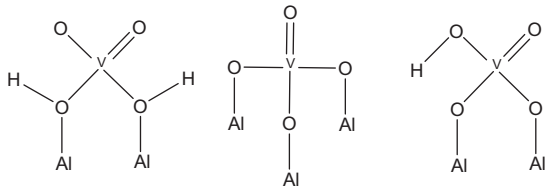

Scheme 1 Schematics of the three unique vanadyl species on alumina characterized by DFT and species-selective Raman spectoscopy [22]. The hydrogen attached to the oxygen not bound to aluminum in the "molecular" species is omitted for clarity.

by a high V_2O_5 loading of 30% that prevents adsorption in addition to partial blockage of channels of alumina by the small agglomerates of V_2O_5 that prevent accessibility for adsorption of ammonia on the active sites [30]. The high acidity of VOx/Al_2O_3-MW may be explained using schematics of Kim et al. [31]. This reveals that the bidentate is the most easily ionized hydroxyl group among the three monomers. The FTIR data also suggest a presence of V═O for materials prepared with the microwave technique. The structure of the molecular monomer (Scheme 1) has two more hydrogen atoms on each of the V–O–Al bridges than the bidentate.

SEM images of alumina, V_2O_5/γ-Al_2O_3-C and V_2O_5/γ-Al_2O_3-MW catalyst are shown in Fig. 6. The particles of γ-Al_2O_3 exhibited fine aggregation of spherical shape and the general appearance of impregnated V_2O_5/γ-Al_2O_3-MW catalysts was somewhat similar to the γ-Al_2O_3 particles. In addition, SEM revealed significant shrinkage of V_2O_5/γ-Al_2O_3-C catalyst resulting in the building of large micron-size particles of the γ-Al_2O_3 after V_2O_5 impregnation. The shrinkage in particle size decreases the size of the voids between them, which is consistent with the minor shift of nitrogen uptake and pore size distribution. Shrinkage of the primary nanocrystal aggregates together with the reduction in micropore volume/surface area in the material reflects the efficient densification of the intermediate nanoparticles [23,32].

The TEM images of alumina, V_2O_5/γ-Al_2O_3-C and V_2O_5/γ-Al_2O_3-MW are shown in Fig. 7. It was found that the particles of V_2O_5/γ-Al_2O_3-MW catalysts were well dispersed and the particle size was less than 10 nm. The TEM images showed that the particles of V_2O_5/γ-Al_2O_3-C appeared to be more agglomerated than the V_2O_5/γ-Al_2O_3-MW samples. The V_2O_5/γ-Al_2O_3-MW had both small separate spherical particles that increased with increasing vanadium loading due to aggregation of their primary particles.

4.2. Catalytic activity

The dehydrogenation of EB was performed at a temperature range from 450 to 600 °C using CO_2 as a mild oxidant in the vapor phase at normal atmospheric pressure over the nano alumina-supported vanadium oxide catalyst.

Among all catalysts examined, the catalysts prepared and treated with MW showed a better catalytic activity in terms of conversion and product selectivity. The observed better activity could be attributed to a high specific surface area (less effect of coke formed on support surface) (Table 1), high metal dispersion, better redox nature and profound acid–base properties of the catalyst. In addition, the deactivation of active site

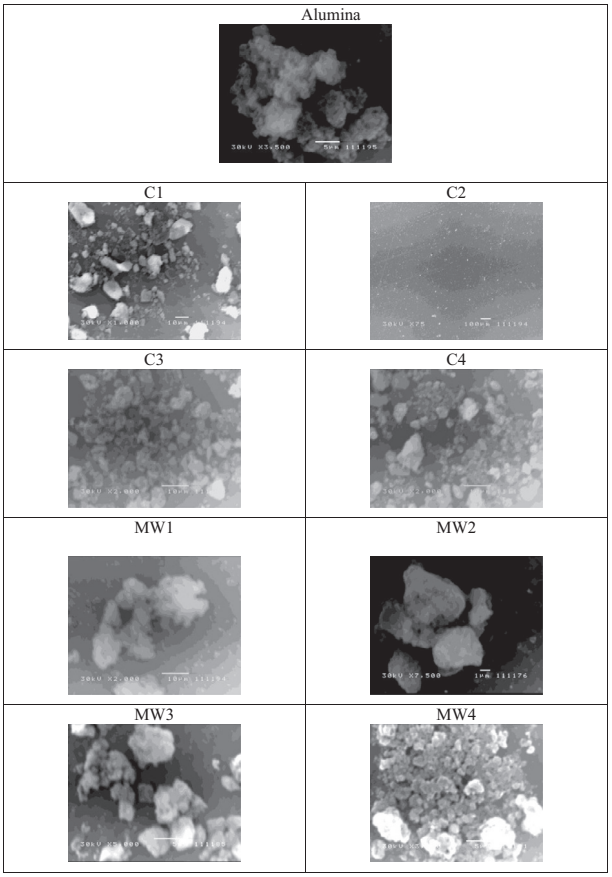

Figure 6 SEM images of the alumina and different prepared catalysts.

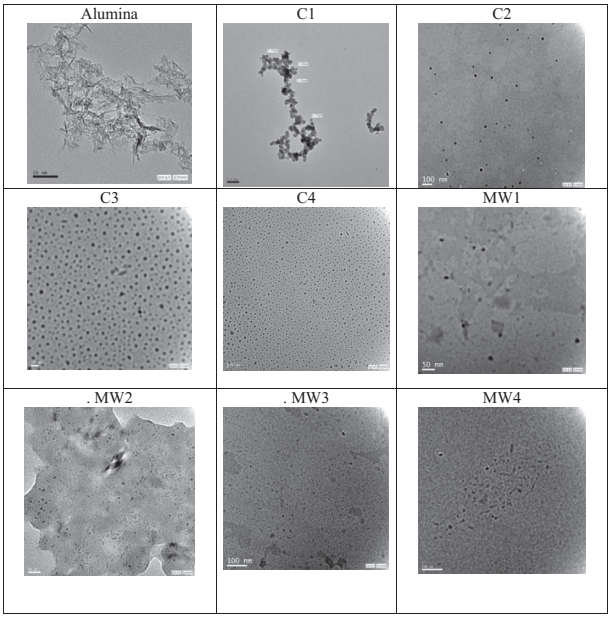

Figure 7 HRTEM images of the alumina and different prepared catalysts.

or mechanism of dehydrogenation on carbon deposits is still complicated [33]. TGA analysis (Table 2) shows the amount of carbon deposit on different catalysts. The MW samples show high amount of carbon than other samples, indicating large coke deposits. Makkee et al. have reported that carbon deposits the catalyzed ethylbenzene dehydrogenation reaction, specially, in the absence of molecular oxygen, which is believed to be oxygen-surface groups like quinones and hydroxyls [34]. Indeed, the low activity of C-catalysts may result from coke formed during reaction, which reduces the activity due to a loss in the available surface area.

Table 2 Acidic values of prepared samples obtained from NH_3-TPD analysis and carbon deposit percent obtained from TGA analysis.

Samples	m mole/g		Carbon deposit (%)
	W	S	
γ-Al_2O_3	0.049	0.445	3
C1- 5% V_2O_5/γ-Al_2O_3	0.166	0.242	3.5
C2- 10% V_2O_5/γ-Al_2O_3	0.059	0.213	7
C3- 20% V_2O_5/γ-Al_2O_3	0.112	0.085	6.2
C4- 30% V_2O_5/γ-Al_2O_3	0.155	0.085	5.6
MW1- 5% V_2O_5/γ-Al_2O_3	0.062	0.457	5.8
MW2- 10% V_2O_5/γ-Al_2O_3	0.080	0.272	11
MW3- 20% V_2O_5/γ-Al_2O_3	0.120	0.289	8.7
MW4- 30% V_2O_5/γ-Al_2O_3	0.177	0.246	7.3

The effect of vanadium loading alumina is shown in Figs. 8 and 9. The catalytic activity of the vanadium oxide/alumina catalysts is strongly dependent on the vanadium loading and the metal oxide support [5,35–38]. EB conversion initially increases with the increase of vanadium content from 5% to 10% and decreases with further vanadium loading. The highest activity for EB dehydrogenation was achieved on the catalyst with a vanadium content of 10%, which has high surface area and large pore size in comparison with other high loadings (Table 1). The pore size of V_2O_5/γ-Al_2O_3-MW is larger than V_2O_5/γ-Al_2O_3-C. Consequently, the transport of products from the pore system and the access to catalytically active sites often play an important role in some diffusion controlled reactions [23,38]. In addition, the high activity of this catalyst could be attributed to the better dispersion of the supported V^{+5} component. The 10%V/alumina catalyst gives an 85.19% conversion of EB with 99.99% selectivity for styrene after 1.0 h on stream. The redox behavior of vanadium oxide plays a key role in EB dehydrogenation with CO_2 over the vanadium oxide-based catalysts, and the effective redox cycle of V occurs only between V^{5+} and V^{4+}. In this cycle styrene formation from EB in the reduction step on V^{5+} containing active site produces a reduced V-site with oxygen vacancy, which is then reoxidized by CO_2. A vanadium component of the catalyst in the steady state practically tends to keep the high oxidation state in the CO_2-EBD reaction [36,39].

When the vanadium loading increased to more than 10% the reduction of V^{+5} species became more difficult due to the formation of multilayer polymeric V_2O_5 species and bulk V_2O_5 over catalyst surface [23,38]. This is seen from the images of Fig. 5. Therefore, the good performance of the catalyst could be related to the mono-dispersion of the isolated and polymeric vanadium oxide species associated with 10% loading, and the synergistic action of alumina and vanadium [23,38,40].

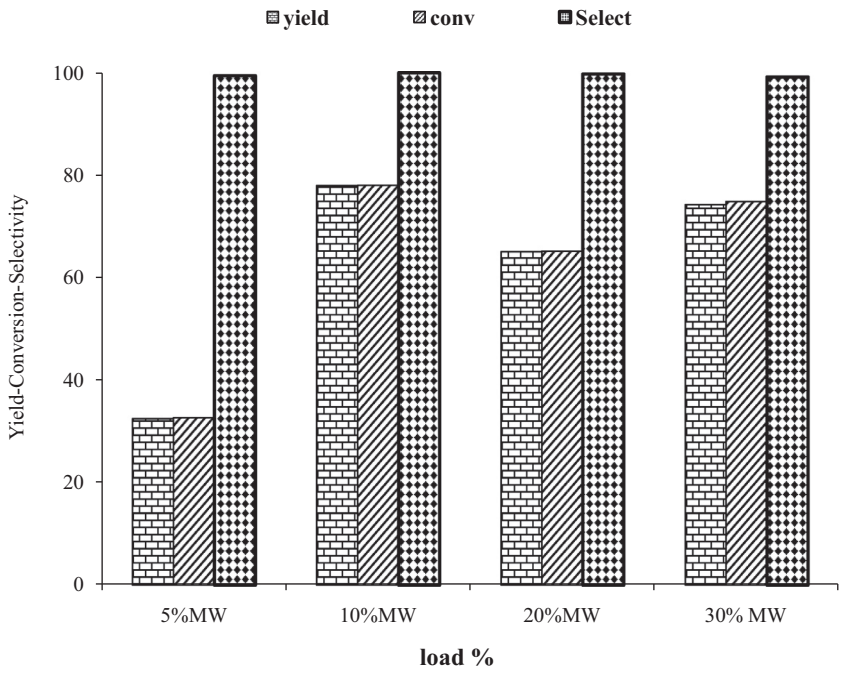

Figure 8 Ethylbenzene conversion, styrene yield and styrene selectivity as a function of load% obtained at 550 °C treated with Microwave.

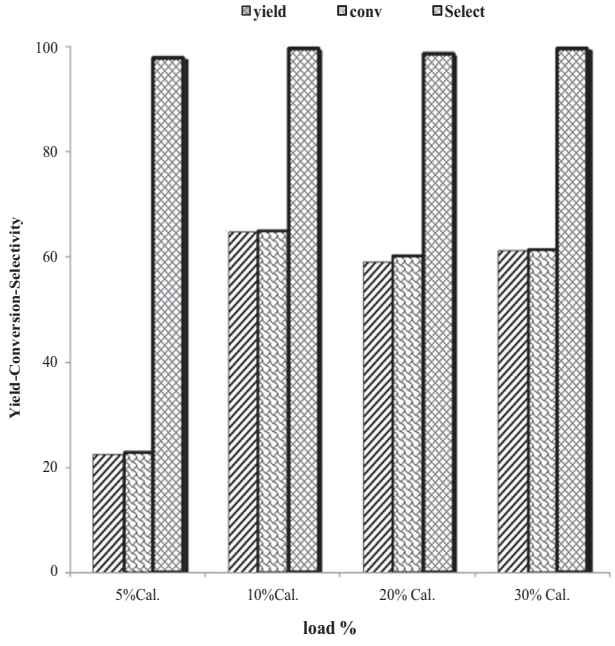

Figure 9 Ethylbenzene conversion, styrene yield and styrene selectivity as a function of load% obtained at 550 °C treated with Calcination.

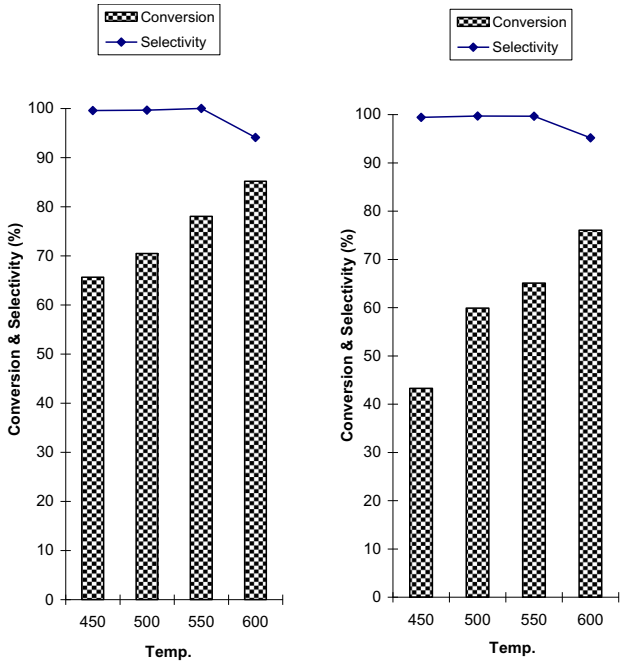

Figure 10 The effect of temperature on ethylbenzene conversion and styrene selectivity (a) catalyst 10% V/alumina MW treated (b) catalyst 10% V/alumina Cal. treated.

The catalytic activity of the 10%V/alumina Cal. is obviously lower than that of 10%V/alumina MW as shown in Fig. 10. The 10%V/alumina MW catalyst gives a 85.19% EB conversion after reaction for 1.0 h, however 10%V/alumina Cal. catalyst gives a 76.03% EB conversion after reaction for 1.0 h. This finding suggests that, with a similar V content, V/alumina MW is superior than V/alumina Cal as a catalyst.

FTIR shows the bidentate vanadium structure is found in samples prepared by microwave due to surface hydroxyl groups bound to the vanadium. Kim et al. have reported that the bidentate structure is more active than the other structures due to the fact that it is less stable by 15 kcal/mol at 550 °C [41]. These calculated results are also consistent with the

observed experimental ordering. The reaction barriers show that the molecular structure would be expected to have high activity for bidentate structures.

5. Conclusions

A series of vanadium-alumina catalysts (5–30 wt%.) were prepared by the solution impregnation method followed by calcinations and microwave treatment. The V/alumina catalysts have high activity for the dehydrogenation of EB to styrene with CO_2. The 10% V_2O_5/γ-Al_2O_3-MW catalyst shows the highest activity. An EB conversion of 85.19% with a styrene selectivity of 99.99% was achieved using this catalyst at 550 °C. EB conversion on the V_2O_5/γ-Al_2O_3-MW catalysts is much higher than that on their conventional V_2O_5/γ-Al_2O_3-C counterparts. Higher conversions can be obtained for EB dehydrogenation with CO_2, which is caused by the oxidative dehydrogenation of EB by oxygen species that originate from CO_2 as well as the coupling of EB simple dehydrogenation with the reverse water–gas shift reaction.

References

[1] I. Serafin, A. Kotarba, M. Grzywa, Z. Sojka, H. Binczycka, P. Kustrowski, J. Catal. 239 (2006) 137–144.
[2] F. Peng, X. Fu, H. Yu, H. Wang, Carbon 45 (2007) 1.
[3] B. Xiang, C. Yu, H. Xu, W. Li, Catal. Lett. 125 (2008) 90–96.
[4] K.N. Rao, B.M. Reddy, B. Abhishek, Y.H. Seo, N. Jiang, S.E. Park, Appl. Catal. B: Environ. 91 (2009) 649–656.
[5] Y. Sakurai, T. Suzaki, K. Nakagawa, N. Ikenaga, H. Aota, T. Suzuki, J. Catal. 209 (2002) 16–24.
[6] M.S. Park, V.P. Vislovskiy, J.S. Chang, Y.G. Shul, J.S. Yoo, S.E. Park, Catal. Tod. 87 (2003) 205–212.
[7] A.L. Sun, Z.F. Qin, S.W. Chen, J.G. Wang, J. Mol. Catal. A: Chem. 210 (2004) 189–195.
[8] W. Li, X. Li, J. Feng, Catal. Lett. 130 (2009) 575–582.
[9] S. Chen, Z.F. Qin, X. Xu, J.G. Wang, Appl. Catal. A: Gen. 302 (2006) 185–192.
[10] R.M. Freire, F.F. de Sousa, A.L. Pinheiro, E. Longhinotti, J.M. Filho, A.C. Oliveira, P.T.C. Freire, A.P. Ayala, A.C. Oliveira, Appl. Catal. A: Gen. 359 (2009) 165–179.
[11] B.S. Liu, R.Z. Chang, L. Jiang, W. Liu, C.T. Au, J. Phys. Chem. C 112 (2009) 15490–15501.
[12] K.N. Rao, B.M. Reddy, S.-E. Park, Appl. Catal. B: Environ. 100 (2010) 472–480.
[13] D. Hong, V.P. Vislovskiy, Y.K. Hwang, S.H. Jhung, J. Chang, Catal. Tod. 131 (2008) 140–145.
[14] B.S. Liu, G. Rui, R.Z. Chang, C.T. Au, Appl. Catal. A 335 (2008) 88–94.
[15] D.Y. Hong, J.S. Chang, J.H. Lee, V.P. Vislovskiy, S.H. Jhung, S.E. Park, Catal. Tod. 112 (2006) 86.
[16] S.W. Chen, Z.F. Qin, A.L. Sun, J.G. Wang, J. Nat. Gas Chem. 15 (2006) 11–20.
[17] V.P. Vislovskiy, J.-S. Chang, M.-S. Park, S.-E. Park, Catal. Commun. 3 (2002) 227–231.
[18] S.M. Solyman, F.Z. Yehia, A. Rabie, Egypt. J. Petrol. 19 (2010) 59–72.
[19] S.J. Bae, S.J. Yoo, Y. Lim, S. Kim, Y. Lim, J. Choi, K.S. Nahm, S.J. Hwang, T.-H. Lim, S.-K. Kim, P. Kim, J. mater. chem. 22 (2012) 8820–8825.
[20] F. Li, K. Xu, Ch. Dong, J. Chen, Front Chem. China 3 (2008) 198–202.
[21] Z. Ramli, S. Chandren, J. Anal. Sci. 11 (2007) 110–116.
[22] K.M. Parida, A.C. Pradhan, J. Das, N. Sahu, Mater. Chem. Phys. 113 (2009) 244–248.
[23] M.A. Betiha, S.A. Mahmoud, M.F. Menoufy, A.M. Al-Sabagh, Appl. Catal. B: Environ. 107 (2011) 316–326.
[24] Z. Wu, S. Dai, H.O. Steven, J. Phys. Chem. C 114 (2010) 412–422.
[25] A.K. Sinha, S.K. Angew, Chem. Ind. Ed. 44 (2005) 271–278.
[26] L. Vradman, M.V. Landau, D. Kantorovich, Y. Koltypin, A. Gedanken, Micropor. Mesopor. Mater. 70 (2005) 307–318.
[27] G.C. Li, S.P. Pang, L. Jiang, Z.Y. Guo, Z.K. Zhang, J. Phys. Chem. B 110 (2006) 9383–9386.
[28] M. Inomata, K. Mori, A. Miyamoto, Y. Murakami, J. Phys. Chem. 87 (1983) 754–761.
[29] J.B. Peri, J. Phys. Chem. 69 (1965) 211–219.
[30] K.U. Nandhini, J.H. Mabel, B. Arabindoo, M. Palanichamy, V. Murugesan, J. Micropor, Mesopor. Mater. 96 (2006) 21–28.
[31] H.S. Kim, S.A. Zygmunt, P.C. Stair, P. Zapol, L.A. Curtiss, J. Phys. Chem. C 113 (2009) 8836–8843.
[32] R. Vidruk, M.V. Landau, M. Herskowitz, V. Ezersky, A. Goldbourt, J. Catal. 282 (2011) 215–227.
[33] C. Nederlof, F. Kapteijn, M. Makkee, Appl. Catal. A: Gen. 417–418 (2012) 163–173.
[34] L.E. Cadus, O.F. Gorriz, J.B. Rivarola, React. Kinet. Catal. Lett. 42 (1990) 101–106.
[35] V.P. Vislovskiy, J.S. Chang, M.S. Park, S.E. Park, Catal Commun. 3 (2002) 227–231.
[36] Y. Sakurai, T. Suzaki, N. Ikenaga, T. Suzuki, Appl. Catal A: Gen 192 (2000) 281–288.
[37] A.L. Sun, Z.F. Qin, S.W. Chen, J.G. Wang, Catal. Tod. 93–95 (2004) 273–279.
[38] M.A. Betiha, H.M.A. Hassan, A.M. Al-Sabagh, A-E.S. Khder, E.A. Ahmed, J. Mater. Chem. 22 (2012) 17551–17559.
[39] J.S. Chang, V.P. Vislovskiy, M.S. Park, D.Y. Hong, J.S. Yoo, S.E. Park, J. Green Chem 5 (2003) 587–590.
[40] L. Zhenhuan, S. Kunmei, B. Cheng, D. Shen, Y. Zhou, Catal. Lett. 135 (2010) 135–140.
[41] H. Kim, G.A. Ferguson, L. Cheng, S.A. Zygmunt, P.C. Stair, L.A. Curtiss, J. Phys. Chem. C 116 (2012) 2927–2932.